Electronic Supporting Information for

Repairing interfacial defect via preferable adsorption of ytterbium for high-utilization and dendrite-free Zn metal anodes

Long Jiang,‡[ab] Zhenyue Xing,‡*[c,d] Yanfen Liu,[c] Xiaodong Shi,[d] Le Li,[ab] Yangyang Liu,[e] Bingan Lu,[f] and Jiang Zhou*[c]

a. State Key Laboratory of Oil and Gas Equipment, CNPC Tubular Goods Research Institute, Xi'an Shaanxi 710077, China.

b. Shaanxi Provincial Key Laboratory of Clean Energy Equipment and Materials, Xi'an Shaanxi 710077, China.

c. School of Materials Science & Engineering, Central South University, Changsha Hunan 410083, China. E-mail: zhou_jiang@csu.edu.cn

d. School of Marine Science and Engineering, State Key Laboratory of Marine Resource Utilization in South China Sea, Hainan University, Haikou Hainan 570228, China. E-mail: xingzy@hainanu.edu.cn

e. State Key Laboratory for Mechanical Behavior of Materials, Xi'an Jiaotong University, Xi'an Shaanxi 710049, China.

f. School of Physics and Electronics, Hunan University, Changsha Hunan 410082, China.

‡These authors contributed equally to this work

Experimental section

Synthesis of $CaV_8O_{20} \cdot xH_2O$

$CaV_8O_{20} \cdot xH_2O$ was prepared by a simple hydrothermal method.[1] 0.81 g V_2O_5 and 0.24 g $CaCO_3$ were added into 50 mL deionized water under continuous magnetic stirring for 0.5 h. Subsequently, the pH value was adjusted to 3 by adding CH_3COOH solution. After stirring for 0.5 h, the mixture was transferred to a 100 mL Teflon-line autoclave and heated at 180 °C for 72 h. The collected products were washed repeatedly with deionized water and then dried at 80 °C for 12 h to obtain the $CaV_8O_{20} \cdot xH_2O$.

Preparation of electrolytes

BE electrolyte (2M $ZnSO_4$) was prepared by dissolving 5.75 g $ZnSO_4 \cdot 7H_2O$ into 10 mL deionized water. 2-0.15Yb electrolyte (2M $ZnSO_4$+0.15M $Yb_2(SO_4)_3$) was prepared by adding 1.17 g $Yb_2(SO_4)_3 \cdot 8H_2O$ into 10 mL BE solution.

Material characterization

Structural characterizations were done by X-ray diffraction using a Rigaku Mini Flex 600 diffractometer. The morphologies and microstructures of samples were performed by scanning electron microscopy (FEI Nova NanoSEM 230, 10 kV) and transmission electron microscopy (JEM-F200, 200 kV) with energy dispersive spectrometer (EDS, Ultim Max 80). The STEM samples were prepared using a focused ion beam (FIB, Helios 5 PFIB). HADDF-STEM imaging and STEM-EDS analysis were conducted by JEOL ARM 200F with JED-2300T. X-ray photoelectron spectroscopy (XPS) was performed using Nexsa X-ray

photoelectron spectrometer (Thermo Scientific). The grain size of deposited Zn was tested by Electron backscattered diffraction (EBSD, Oxford instruments Nordly Max3). The three-dimensional morphology of the Zn anode surface was performed using a Laser confocal scanning microscope (LCSM, KEYENCE CK-X1000). The in-situ optical photographs were taken with an optical microscope (LeicaDM2700M). Electron probe microanalysis (EPMA) was carried out on a JXA-8230 instrument with wavelength-dispersive X-ray spectroscopy characterization.

Electrochemical measurements

The cathode was obtained by pressing the mixture of $CaV_8O_{20} \cdot xH_2O$, conductive carbon black, and PVDF at a mass ratio of 7:2:1 on the stainless-steel mesh. The Zn foil was punched into disks (15 mm). The glass fiber film was used as the separator (19 mm). Cyclic voltammetry (CV), electrochemical impedance spectroscopy (EIS), and Tafel plots were measured on an electrochemical workstation (CHI 660E, China). Different from ordinary coin cells, graphite felt was used as a current collector to increase the mass loading of cathode in CVO|Zn cells at a low N/P of 2.26, where the mass of CVO cathode is about 4.8 mg cm^{-2} with the capacity of 2.85 mA h, while Zn foil with the thickness of 10 μm was used as anode. The CVO|Zn pouch cell was fabricated by stacked technology with three Zn foils and three pieces of CVO electrodes. The cathode was prepared by coating the slurry mixture on a carbon felt current collector with a size of 10 cm × 8 cm × 3 mm. Before the cycling test, the assembled pouch cell was activated five times at 80 mA g$_{cathode}$$^{-1}$.

Density functional theory (DFT) calculations

DFT calculations were performed on the CP2K package by using the CP2K package mixed Gaussian and plane-wave scheme and the Quickstep module, with the help of Multiwfn software. The Perdew-Burke-Ernzerhof (PBE) exchange-correlation functional, Goedecker-Teter-Hutter (GTH) pseudopotential was used to describe the system. A plane-wave energy cut-off and relative cut-off of 400 Ry and 55 Ry have been employed, respectively. The energy convergence criterion was set to 10^{-6} Hartree. The DFT-D3 level correction for dispersion interactions was applied. A geometry optimization was considered convergent when the energy change was smaller than 0.011 eV Å^{-1}.

Finite element simulation

A 2D finite element model was established to demonstrate the current density distribution at the interface of electrolyte/anode with different electrolytes to predict the Zn^{2+} ion deposition process, which was investigated by COMSOL Multiphysics 5.6 framework coupling with the tertiary current distribution and Nernst-Planck physics module. The geometric models are shown in Fig. S21. The ionic conductivity of electrolytes was 1.34 S m^{-1} and 1.01 S m^{-1}, respectively.
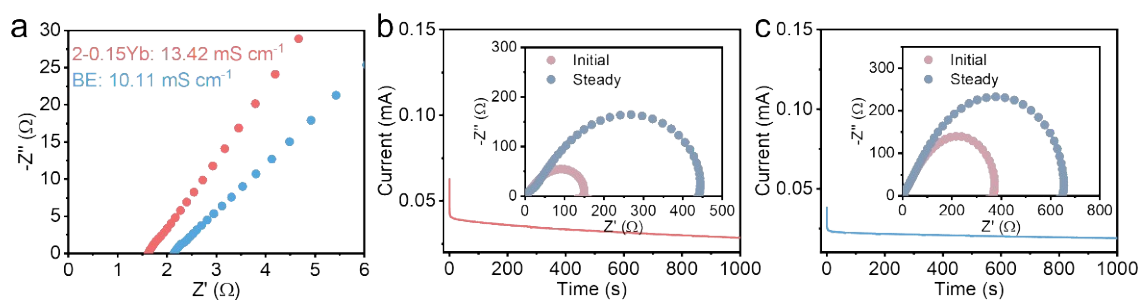
Figures

Fig. S1 (a) Ionic conductivity. Zinc ion transference number of (b) 2-0.15Yb and (c) BE electrolyte.
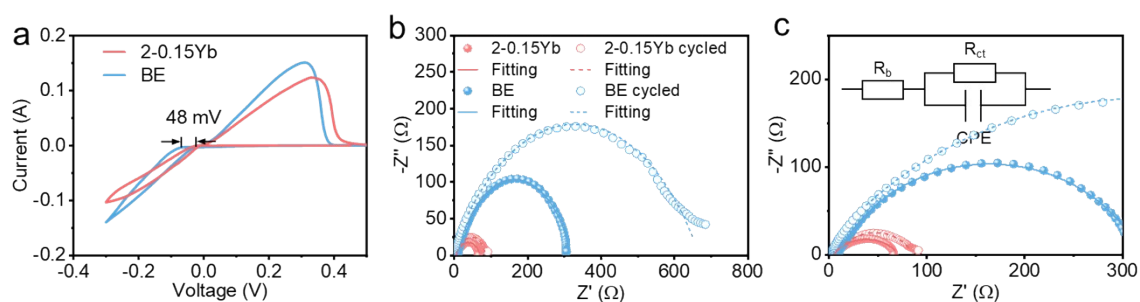

Fig. S2 (a) CV curves of Zn|Cu cells. (b) EIS curves and (c) corresponding partial enlargement EIS curves of Zn|Zn symmetric cells before and after 30 cycles at 2 mA cm^{-2} and 2 mA h cm^{-2} (inset is the equivalent circuit diagram).
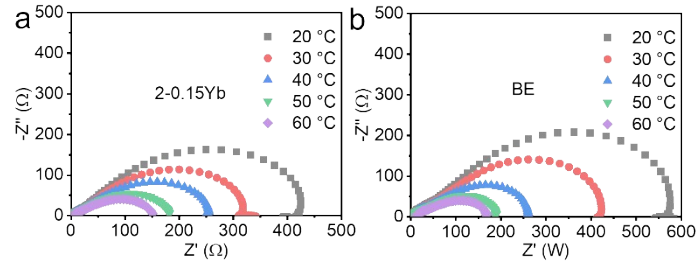
Fig. S3 EIS of symmetric cells with (a) 2-0.15Yb and (b) BE electrolyte under different

temperatures.

The activation energy (E_a) is calculated from equation (1).[2]

$$\frac{1}{R_{ct}} = A\exp\frac{-E_a}{RT} \tag{1}$$

Where R_{ct} represents the charge transference impedance, A is Arrhenius constant, R and

T are gas constant and temperature constant, respectively.
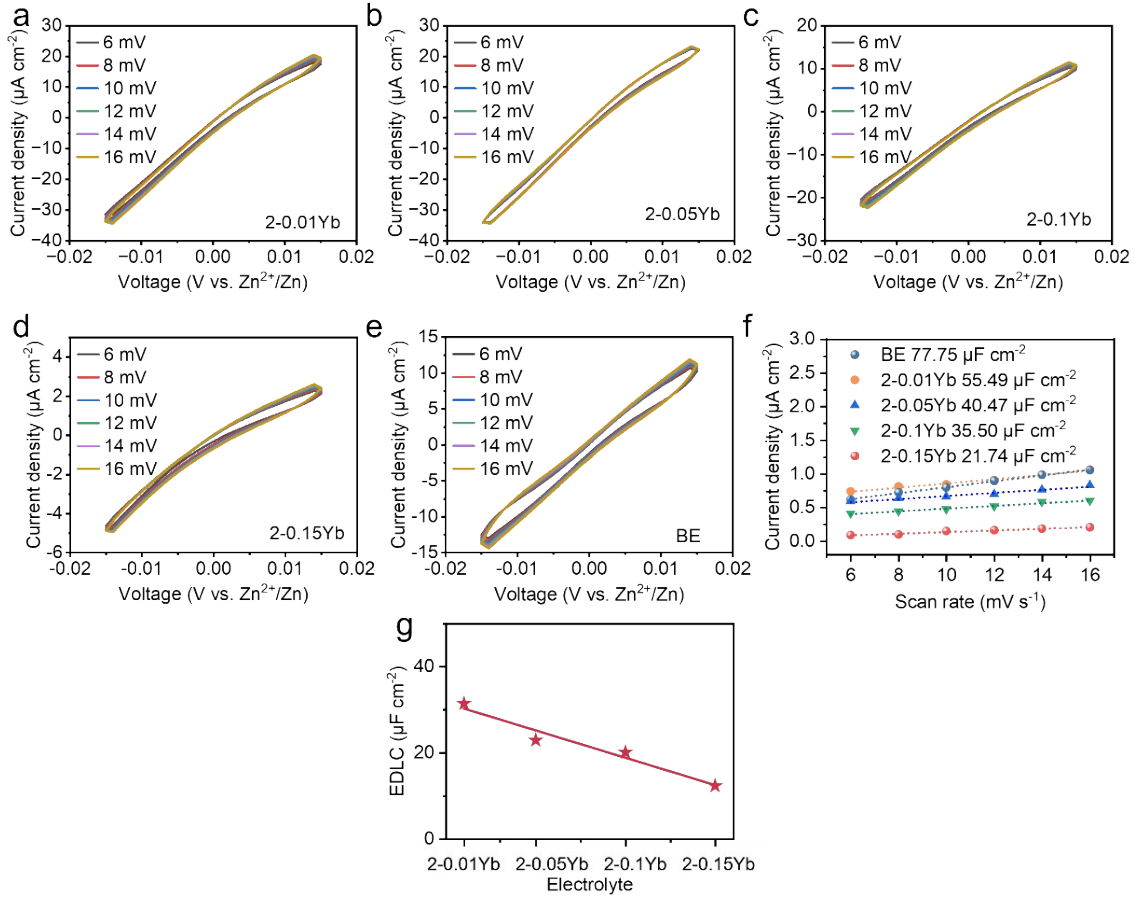
Fig. S4 CV curves of symmetric cells with (a) 2-0.01Yb, (b) 2-0.05Yb, (c) 2-0.1Yb, (d) 2-0.15Yb and (e) BE electrolyte under various scan rates. (f) Double layer capacitance at Zn anodes in different electrolytes. (g) Relationship between the values of EDLC and electrolytes with different concentrations.

The electric double layer capacitance (EDLC) is obtained by equation (2).[3]

$$C = \frac{i}{v} \tag{2}$$

Where C is capacitance, v is scanning rate, i is current density, the value of i is determined by taking the half of the current density difference between positive and negative scan under each scanning rate.
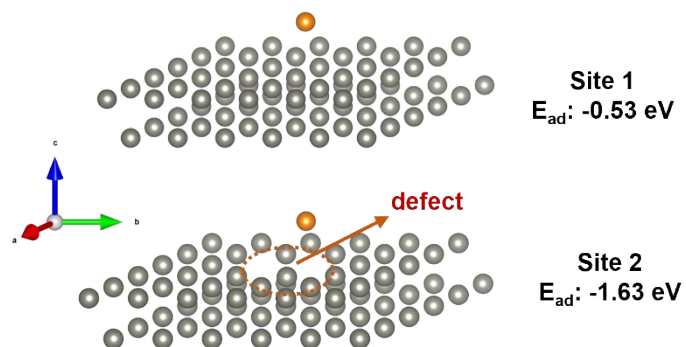
Fig. S5 Adsorption energies between Zn^{2+} and Zn anode at different sites.
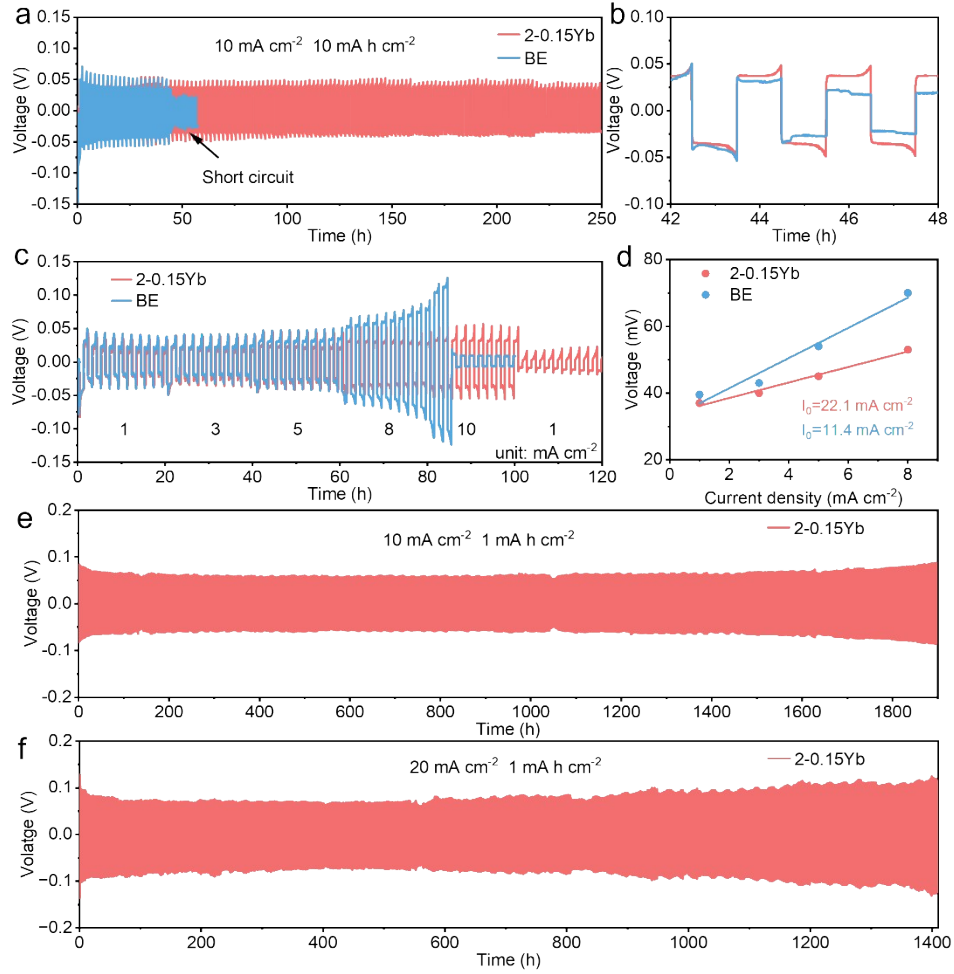
Fig. S6 (a) Cyclic performance and (b) local magnification of symmetric cells at 10 mA cm^{-2}.

(c) Rate performance of symmetric cells. (d) Exchange current densities. Cyclic performance

of symmetric cells at (e)10 mA cm^{-2} and (f) 20 mA cm^{-2} with an areal capacity of 1 mA h

cm^{-2}.

Exchange current density can be calculated by Equation (3).[4]

$$i = i_0 \frac{F\eta}{2RT} \tag{3}$$

where i is current density, i_0 is the exchange current density, F and R are Faradic

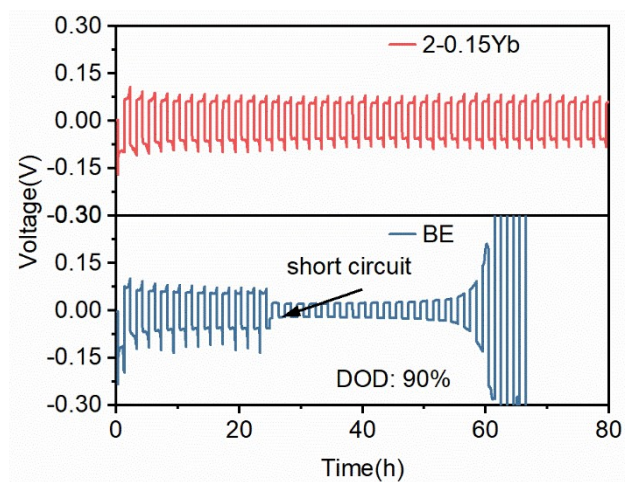constant and gas constant, respectively, T is temperature constant and η is overpotential.

Fig. S7 Galvanostatic Zn^{2+} plating/stripping in Zn|Zn symmetric cells under the DOD of
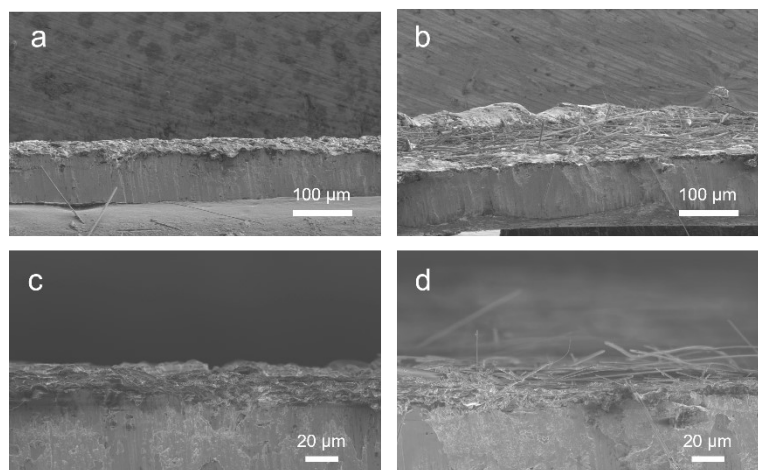
90%.

Fig. S8 Cross-section SEM images of Zn anodes deposited at 10 mA cm^{-2} for 1h in (a, c)
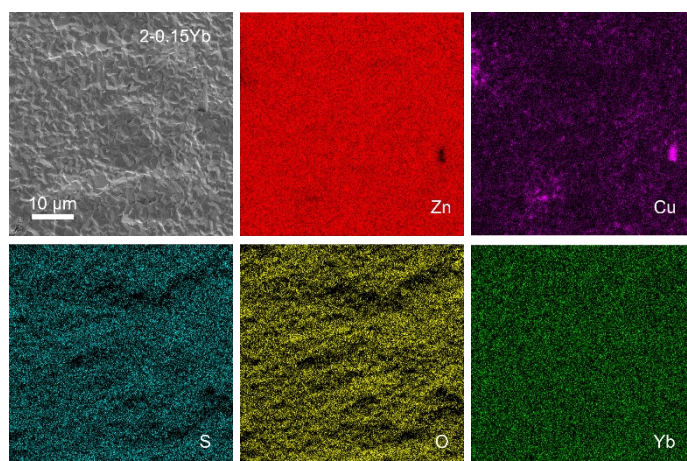
2-0.15Yb and (b, d) BE electrolyte.

Fig. S9 SEM images and EDS maps of Cu foils with the plating capacity of 1 mA h cm^{-2} in 2-0.15Yb electrolyte.
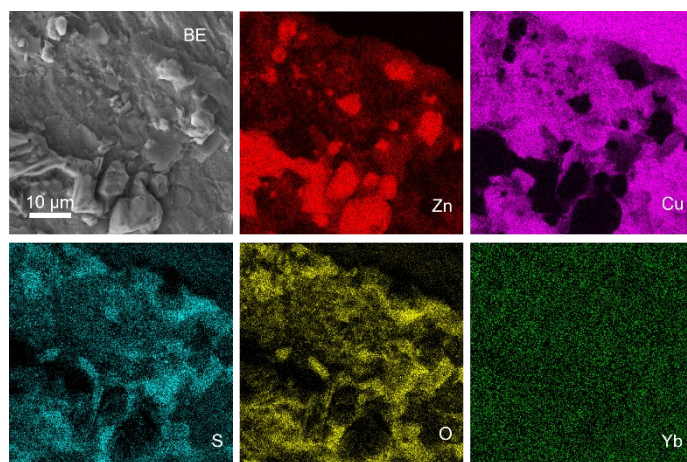

Fig. S10 SEM images and EDS maps of Cu foils with the plating capacity of 1 mA h cm^{-2} in BE electrolyte.

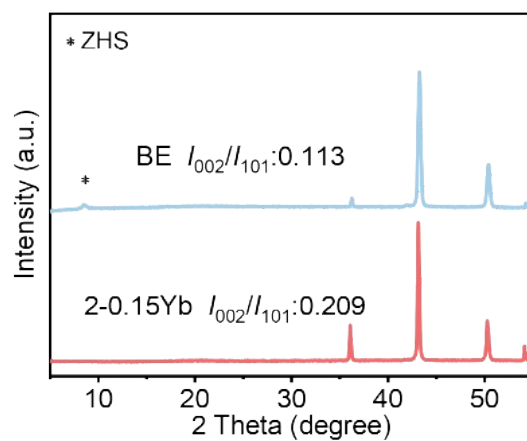**Fig. S11** XRD of Cu foils with the plating capacity of 1 mA h cm^{-2} at 5 mA cm^{-2} in different electrolytes.
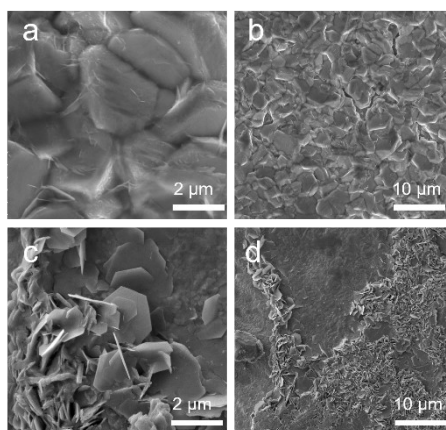
Fig. S12 SEM images of Cu foils with the plating capacity of 1 mA h cm^{-2} at 5 mA cm^{-2} in (a, b) 2-0.15Yb and (c, d) BE electrolytes.
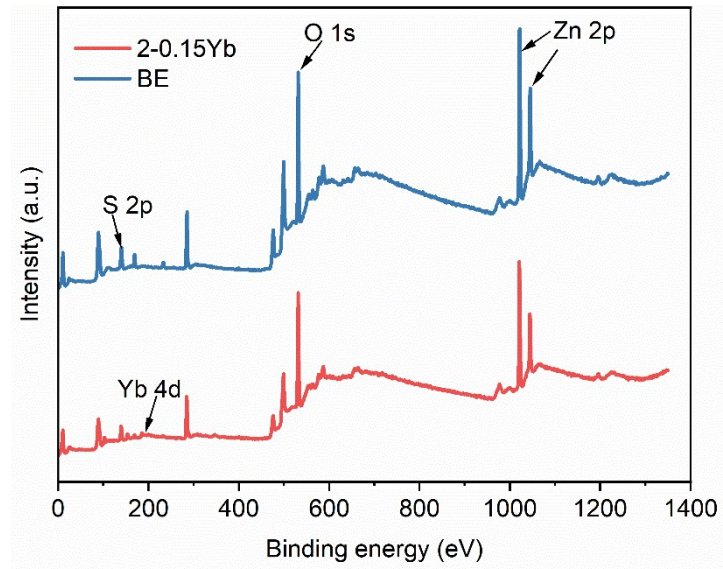
Fig. S13 XPS spectra of Zn anodes after cycling.
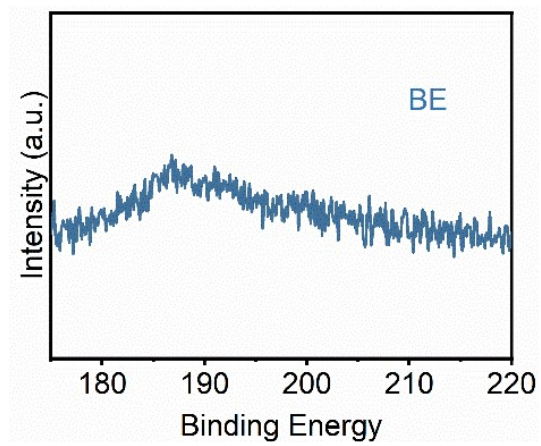
Fig. S14 XPS spectra for Yb 4d of Zn anode after cycling in BE electrolyte.
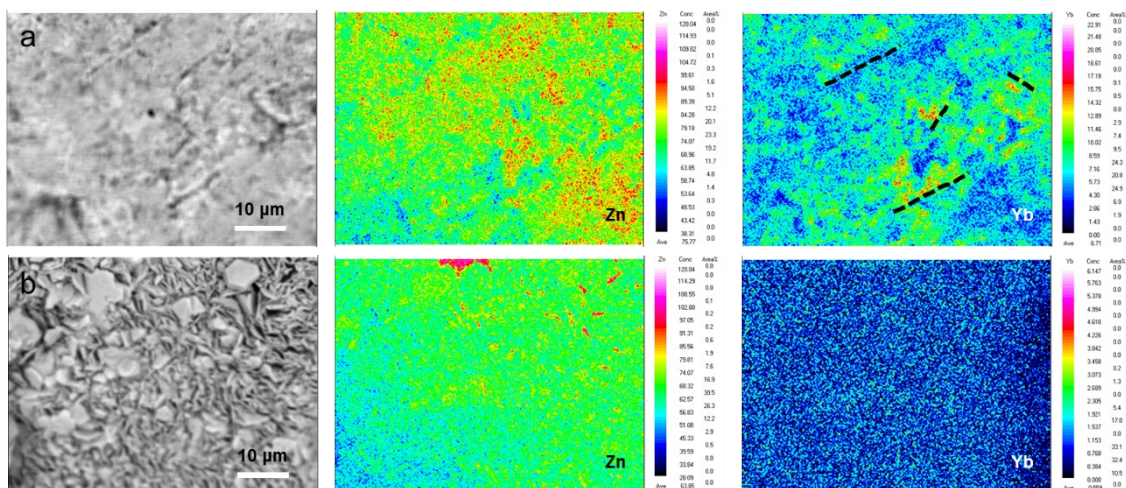
Fig. S15 Morphology and corresponding EPMA mapping of Zn anodes after cycling in (a) 2-0.15Yb electrolyte and (b) BE electrolyte.
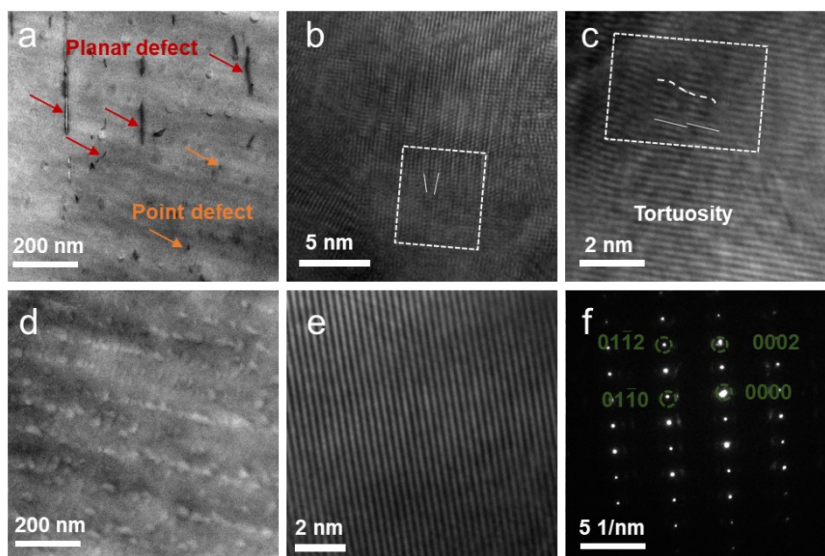
Fig. S16 (a) HAADF and (b, c) HRTEM images of Zn electrodeposit in BE electrolyte. (d) HAADF, (e) HRTEM image and (f) SAED pattern of Zn electrodeposit in 2-0.15Yb electrolyte.
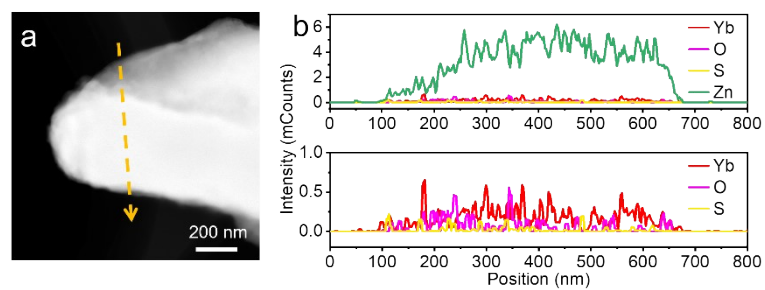
Fig. S17 (a) HAADF and (b) corresponding linear EDS results of Zn anode after 10 cycles in 2-0.15Yb.
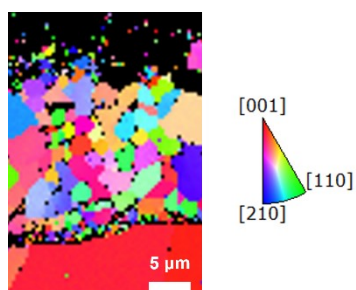
Fig. S18 EBSD IPF mapping of Zn anode after plating in 2-0.15Yb electrolytes.

Site	Yb (Wt%/At%)
1	1.22/0.47
2	1.56/0.6
3	1.55/0.59
4	2.67/1.03
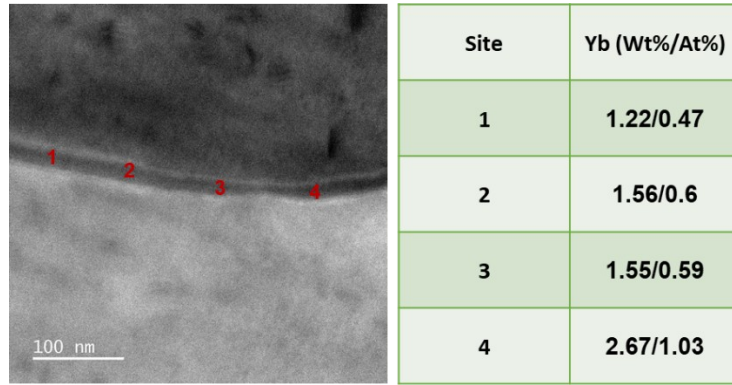
Fig. S19 HADDF image of a typical grain boundary in Zn deposit with 2-0.15Yb and the corresponding EDS analysis of Yb concentration for the 4 positions along the grain boundary.
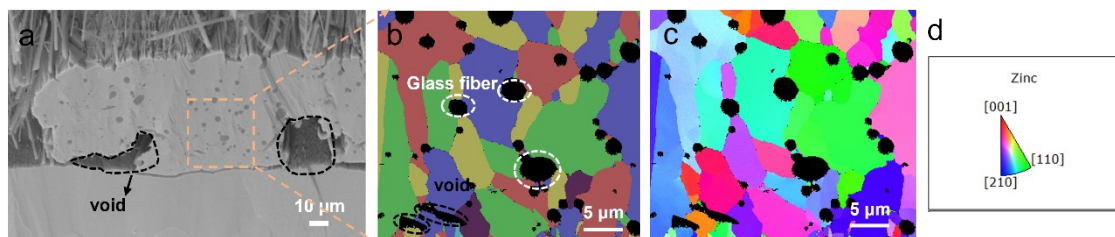
Fig. S20 (a) Section SEM image, (b) EBSD mapping, and (c, d) IPF mapping of Zn anode after plating in BE electrolyte with a capacity of 10 mA h cm^{-2} at 10 mA cm^{-2}.
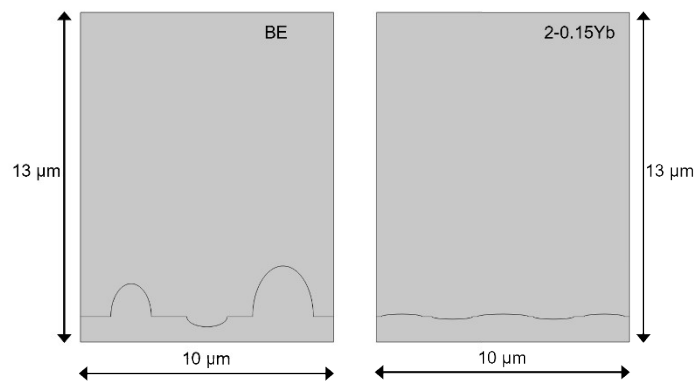
Fig. S21 Models for Zn anodes with BE and 2-0.15Yb electrolytes.
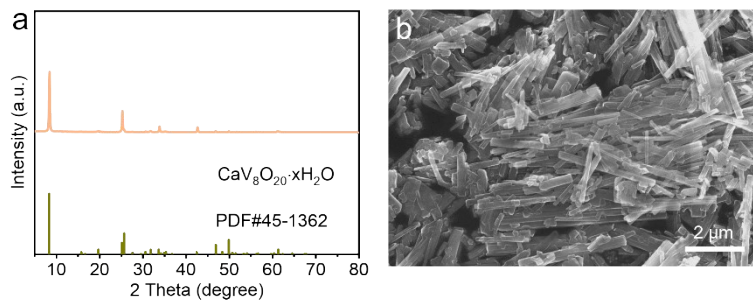
Fig. S22 (a) XRD and (b) SEM image of CVO material.
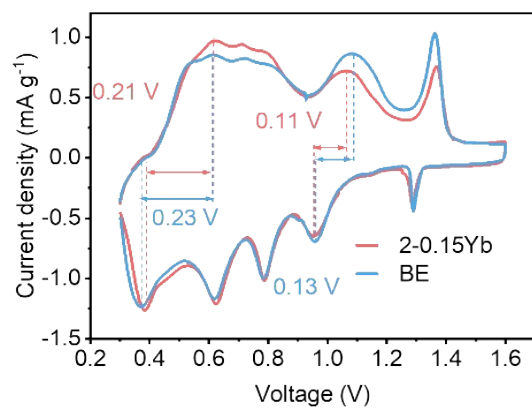
Fig. S23 CV curves CVO|Zn cells with different electrolytes at 0.5 mV s^{-1}.
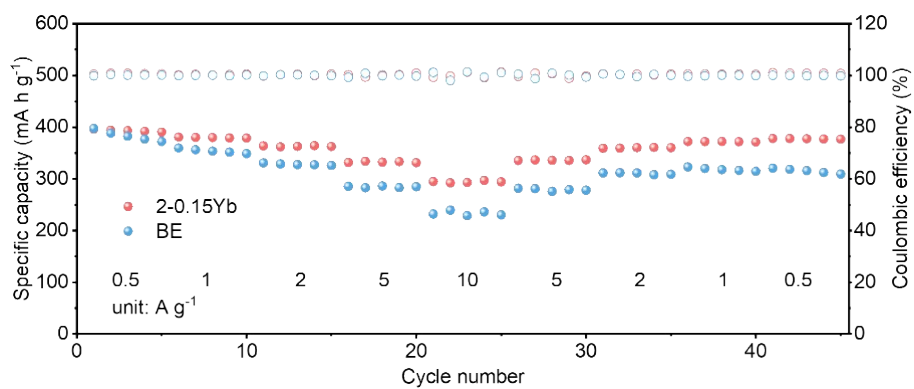
Fig. S24 Rate performance of CVO|Zn cells with different electrolytes.
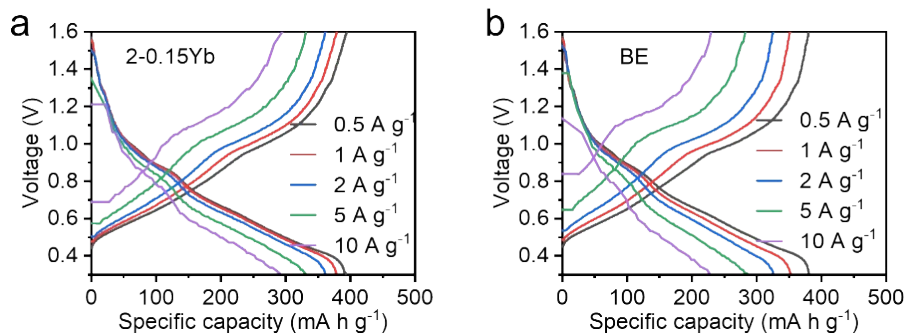
Fig. S25 GVD curves of CVO|Zn cells at different electrolytes.

Table. S1 Calculation results of $t_{Zn^{2+}}$ of different electrolytes.

Electrolyte	R_I (Ω)	R_S (Ω)	I_I (μA)	I_S (μA)	t
2-0.15Yb	144.2	446.4	62.8	28.6	0.69
BE	376.1	640.5	38.2	19.0	0.36

Table. S2 Summary of electrochemical performance of recent Zn anode with different strategies.

Strategies	Current density (mA cm^{-2})	Areal capacity (mA h cm^{-2})	CPC (mA h cm^{-2})	DOD$_{Zn}$(%)/ Time (h)	Ref.
2-0.15Yb	**1**	**1**	**2400**		**This work**
	10	**10**	**2500**		
	10	**1**	**19000**		
	20	**1**	**28000**		
				80/125	
La^{3+}-ZS	1	1	1200		5
2Zn-1Sc	4	4	520		6
ZLT-DMC	1	1	2000		7
HSE-10 m	0.5	0.5	600		8
Zn-Tx	0.5	0.5	600		9
KL-Zn	0.2	0.1	440		10
Zn@Ag	0.5	0.5	300		11
	5	5	550		
Zn(0002)	10	2	5400		12
Zn$_5$Cu	1		1000		13
PSPMA	1	0.5	1100		14
PS-Zn	5	1	5000		15
	10	1	5000		
ZnSO$_4$-SrTiO$_3$	1	0.5	2000		16
ZS-C4	20	10	6000		17
CP/EGZn/Betaine	0.5	0.5	1000		18
1M Zn(PS)$_2$+0.2 TBATS	1	1	2000		19
Co(TAPC)/ZnSO$_4$	20	5	2500		20
4 m Zn(BF$_4$)$_2$/EG	0.5	0.25	2000		21
				50/200	
PVDF-Sn	1	1	1200		22
HPA	20	5	6000		23
ZnSO$_4$-C$_3$N$_4$QDs	1	1	1200		24
ZIG-20 wt%	1	0.5	900		25
IL-AE	1	1	700		26

2M ZnSO$_4$+50 mM DOTf	4	4	1400		27
β-CD	1	1	500		28
Cu/Zn-N/P-CMFs	2	2	1200		29
α-CD+ZnSO$_4$	10	1	1600	30/200	30
(002)-Zn	2	2	1000		31
SFPAM-Zr	0.5	0.5	1250		32
1Z-5H	1	1	1500		33
	20	4	1400		
25% SL				80/50	34
D-ZF				60/40	35
ZSO/DM-0.09				45.54/135	36

Table. S3 Comparison of the cycling performance of Zn|2-0.15Yb|CVO pouch cell with previously reported pouch cells.

Strategies	Cathode	Current density (mA g^{-1})	Capacity (A h)	Cycle number	Capacity retention (%)	Ref.
2-0.15Yb	**CaV$_8$O$_{20}$·xH$_2$O**	**80**	**0.83**	**63**	**79**	**This work**
DMI	PANI	50	0.028	75	86.9	37
PSE	LiMn$_2$O$_4$	~	0.035	~	~	38
ZSO/DM-0.09	NH$_4$V$_4$O$_{10}$	250	0.037	50	92	36
N-ac/ZSO	ZnV$_6$O$_{16}$·8H$_2$O	474	0.04	100	90.1	39
β-CD	Zn$_x$V$_2$O$_5$	500	0.043	100	90.6	40
QEE	MnO$_2$	300	0.011	100	79	41
101-Zn	MnO$_2$	100	0.033	50	87.3	42
Zn-plated PBA@CC	PANI-intercalated V$_2$O$_5$	500	~	50	71	43
Zn@Bi/Bi$_2$O$_3$	MnO$_2$	12	0.002	100	84.1	44
ZnO(002)@Zn	V$_2$O$_5$	500	0.09	~	~	45
Fs-Zn	MnO$_2$	200	0.047	40	76.5	46
ZnSO4-SrTiO$_3$	MnO$_2$	500	~	50	80	16
Zn@ZSO	K$_{0.27}$MnO$_2$·0.54H$_2$O	308	0.5	50	86.3	47
Zn@ZBO	MnO$_2$	154	0.075	100	73.7	48

References

1 L. Zhang, X. Qin, L. Wang, Z. Zhao, L. Mi and Q. Lu, *Front. Chem. Sci. Eng.*, 2023, **17**, 1244-1253.

2 S. R. Jin, F. X. Duan, X. Y. Wu, J. P. Li, X. X. Dan, X. X. Yin, K. N. Zhao, Y. J. Wei, Y. M. Sui, F. Du and Y. Z. Wang, *Small*, 2022, **18**, 2205462.

3 B. Niu, Z. Li, D. Luo, X. Ma, Q. Yang, Y.-E. Liu, X. Yu, X.-r. He, Y. Qiao and X. Wang, *Energy Environ. Sci.*, 2023, **16**, 1662-1675.

4 P. Cao, X. Zhou, A. Wei, Q. Meng, H. Ye, W. Liu, J. Tang and J. Yang, *Adv. Funct. Mater.*, 2021, **31**, 2100398.

5 R. Zhao, H. Wang, H. Du, Y. Yang, Z. Gao, L. Qie and Y. Huang, *Nat. Commun.*, 2022, **13**, 3252.

6 M. Kim, S. J. Shin, J. Lee, Y. Park, Y. Kim, H. Kim and J. W. Choi, *Angew. Chem. Int. Ed.*, 2022, **61**, e202211589.

7 H. Jiang, L. Tang, Y. Fu, S. Wang, S. K. Sandstrom, A. M. Scida, G. Li, D. Hoang, J. J. Hong, N.-C. Chiu, K. C. Stylianou, W. F. Stickle, D. Wang, J. Li, P. A. Greaney, C. Fang and X. Ji, *Nat. Sustain.*, 2023, **6**, 806-815.

8 D. Dong, T. Wang, Y. Sun, J. Fan and Y.-C. Lu, *Nat. Sustain.*, 2023, **6**, 1474-1484.

9 Y. Zhang, S. Shen, K. Xi, P. Li, Z. Kang, J. Zhao, D. Yin, Y. Su, H. Zhao, G. He and S. Ding, *Angew. Chem. Int. Ed.*, 2024, e202407067.

10 C. Zhou, Z. Wang, Q. Nan, H. Wen, Z. Xu, J. Zhang, Z. Zhao, J. Li, Z. Xing, P. Rao, Z. Kang, X. Shi and X. Tian, *Angew. Chem. Int. Ed.*, 2024, e202412006.

11 X. Zhou, B. Wen, Y. Cai, X. Chen, L. Li, Q. Zhao, S. L. Chou and F. Li, *Angew.*

Chem. Int. Ed., 2024, **63**, e202402342.

12   X. Zhang, J. Li, Y. Liu, B. Lu, S. Liang and J. Zhou, *Nat. Commun.*, 2024, **15**, 2735.

13   H. Tian, G. Feng, Q. Wang, Z. Li, W. Zhang, M. Lucero, Z. Feng, Z. L. Wang, Y. Zhang, C. Zhen, M. Gu, X. Shan and Y. Yang, *Nat. Commun.*, 2022, **13**, 7922.

14   H. Liu, Q. Ye, D. Lei, Z. Hou, W. Hua, Y. Huyan, N. Li, C. Wei, F. Kang and J. Wang, *Energy Environ. Sci.*, 2023, **16**, 1610-1619.

15   Q. Li, A. Chen, D. Wang, Y. Zhao, X. Wang, X. Jin, B. Xiong and C. Zhi, *Nat. Commun.*, 2022, **13**, 3699.

16   R. Deng, Z. He, F. Chu, J. Lei, Y. Cheng, Y. Zhou and F. Wu, *Nat. Commun.*, 2023, **14**, 4981.

17   Z. Hu, F. Zhang, F. Wu, H. Wang, A. Zhou, Y. Chen, T. Xue, R. Chen and L. Li, *Energy Environ. Sci.*, 2024, **17**, 4794-4802.

18   Q. J. Fu, S. W. Hao, X. R. Zhang, H. A. Zhao, F. Xu and J. Yang, *Energy Environ. Sci.*, 2023, **16**, 1291-1311.

19   S. Chen, D. Ji, Q. Chen, J. Ma, S. Hou and J. Zhang, *Nat. Commun.*, 2023, **14**, 3526.

20   K. Zhu, C. Guo, W. Gong, Q. Xiao, Y. Yao, K. Davey, Q. Wang, J. Mao, P. Xue and Z. Guo, *Energy Environ. Sci.*, 2023, **16**, 3612-3622.

21   D. Han, C. Cui, K. Zhang, Z. Wang, J. Gao, Y. Guo, Z. Zhang, S. Wu, L. Yin, Z. Weng, F. Kang and Q.-H. Yang, *Nat. Sustain.*, 2022, **5**, 205-213.

22   Q. Cao, Y. Gao, J. Pu, X. Zhao, Y. Wang, J. Chen and C. Guan, *Nat. Commun.*, 2023, **14**, 641.

23   Z. Yang, Y. Sun, S. Deng, H. Tong, M. Wu, X. Nie, Y. Su, G. He, Y. Zhang, J. Li and

G. Chai, *Energy Environ. Sci.*, 2024, **17**, 3443-3453.

24   W. Zhang, M. Dong, K. Jiang, D. Yang, X. Tan, S. Zhai, R. Feng, N. Chen, G. King, H. Zhang, H. Zeng, H. Li, M. Antonietti and Z. Li, *Nat. Commun.*, 2022, **13**, 5348.

25   Y. Wang, Q. Li, H. Hong, S. Yang, R. Zhang, X. Wang, X. Jin, B. Xiong, S. Bai and C. Zhi, *Nat. Commun.*, 2023, **14**, 3890.

26   L. Yu, J. Huang, S. Wang, L. Qi, S. Wang and C. Chen, *Adv. Mater.*, 2023, **35**, e2210789.

27   C. Li, A. Shyamsunder, A. G. Hoane, D. M. Long, C. Y. Kwok, P. G. Kotula, K. R. Zavadil, A. A. Gewirth and L. F. Nazar, *Joule*, 2022, **6**, 1103-1120.

28   M. Qiu, P. Sun, Y. Wang, L. Ma, C. Zhi and W. Mai, *Angew. Chem. Int. Ed.*, 2022, **61**, e202210979.

29   Y. Zeng, Z. Pei, D. Luan and X. W. D. Lou, *J. Am. Chem. Soc.*, 2023, **145**, 12333-12341.

30   K. Zhao, G. Fan, J. Liu, F. Liu, J. Li, X. Zhou, Y. Ni, M. Yu, Y. M. Zhang, H. Su, Q. Liu and F. Cheng, *J. Am. Chem. Soc.*, 2022, **144**, 11129-11137.

31   J. Zhang, W. Huang, L. Li, C. Chang, K. Yang, L. Gao and X. Pu, *Adv. Mater.*, 2023, **35**, e2300073.

32   Y. Cheng, Y. Jiao and P. Wu, *Energy Environ. Sci.*, 2023, **16**, 4561-4571.

33   M. Kim, J. Lee, Y. Kim, Y. Park, H. Kim and J. W. Choi, *J. Am. Chem. Soc.*, 2023, **145**, 15776-15787.

34   M. Wang, J. Ma, Y. Meng, J. Sun, Y. Yuan, M. Chuai, N. Chen, Y. Xu, X. Zheng, Z. Li and W. Chen, *Angew. Chem. Int. Ed.*, 2023, **62**, e202214966.

35   J. Li, Z. Guo, J. Wu, Z. Zheng, Z. Yu, F. She, L. Lai, H. Li, Y. Chen and L. Wei, *Adv. Energy Mater.*, 2023, **13**, 2301743.

36   S. Zhou, X. Meng, Y. Chen, J. Li, S. Lin, C. Han, X. Ji, Z. Chang and A. Pan, *Angew. Chem. Int. Ed.*, 2024, **63**, e202403050.

37   R. Yao, Y. Zhao, L. Wang, C. Xiao, F. Kang, C. Zhi and C. Yang, *Energy Environ. Sci.*, 2024, **17**, 3112-3122.

38   A. Chen, Y. Zhang, Q. Li, G. Liang, S. Yang, Z. Huang, Q. Yang, H. Hu, X. Li, Z. Chen, J. Fan and C. Zhi, *Energy Environ. Sci.*, 2023, **16**, 4054-4064.

39   D. Xu, X. Ren, H. Li, Y. Zhou, S. Chai, Y. Chen, H. Li, L. Bai, Z. Chang, A. Pan and H. Zhou, *Angew. Chem. Int. Ed.*, 2024, **63**, e202402833.

40   J. Luo, L. Xu, Y. Yang, S. Huang, Y. Zhou, Y. Shao, T. Wang, J. Tian, S. Guo, J. Zhao, X. Zhao, T. Cheng, Y. Shao and J. Zhang, *Nat. Commun.*, 2024, **15**, 6471.

41   Y. Hu, Z. Liu, L. Li, S. Guo, X. Xie, Z. Luo, G. Fang and S. Liang, *Natl. Sci. Rev.*, 2023, **10**, nwad220.

42   Z. Liu, Z. Guo, L. Fan, C. Zhao, A. Chen, M. Wang, M. Li, X. Lu, J. Zhang, Y. Zhang and N. Zhang, *Adv. Mater.*, 2023, **36**, 202305988.

43   D. Deng, K. Fu, R. Yu, J. Zhu, H. Cai, X. Zhang, J. Wu, W. Luo, L. Mai, *Adv. Mater.*, 2023, **35**, 2302353.

44   X. Tian, Q. Zhao, M. Zhou, X. Huang, Y. Sun, X. Duan, L. Zhang, H. Li, D. Su, B. Jia and T. Ma, *Adv. Mater.*, 2024, **36**, 2400237.

45   C. Yang, P. Woottapanit, S. Geng, K. Lolupiman, X. Zhang, Z. Zeng, G. He and J. Qin, *Adv. Mater.*, 2024, **36**, 2408908.

46   S. Lian, Z. Cai, M. Yan, C. Sun, N. Chai, B. Zhang, K. Yu, M. Xu, J. Zhu, X. Pan, Y. Dai, J. Huang, B. Mai, L. Qin, W. Shi, Q. Xin, X. Chen, K. Fu, Q. An, Q. Yu, L. Zhou, W. Luo, K. Zhao, X. Wang and L. Mai, *Angew. Chem. Int. Ed.*, 2024, **63**, e202406292.

47   R. Guo, X. Liu, F. Xia, Y. Jiang, H. Zhang, M. Huang, C. Niu, J. Wu, Y. Zhao, X. Wang, C. Han and L. Mai, *Adv. Mater.*, 2022, **34**, e2202188.

48   D. Wang, H. Liu, D. Lv, C. Wang, J. Yang and Y. Qian, *Adv. Mater.*, 2022, **35**, e2207908.